

# **SIMULATING FIRE WHIRLS**

by

**Francine Battaglia, Kevin B. McGrattan,  
Ronald G. Rehm and Howard R. Baum  
Building and Fire Research Laboratory  
National Institute of Standards and Technology  
Gaithersburg, MD 20899 USA**

Reprinted from *Combustion Theory Modelling*, Vol. 4, 123-138, 2000.

**NOTE:** This paper is a contribution of the National Institute of Standards and Technology and is not subject to copyright.



**NIST**

**National Institute of Standards and Technology**  
Technology Administration, U.S. Department of Commerce

## Simulating fire whirls

Francine Battaglia†§, Kevin B McGrattan‡, Ronald G Rehm‡ and Howard R Baum‡

† Mechanical Engineering Department, Iowa State University, Ames, IA 50011, USA

‡ National Institute of Standards and Technology, Gaithersburg, MD 20899, USA

E-mail: francine@iastate.edu

Received 19 May 1999, in final form 1 February 2000

**Abstract.** A numerical investigation of swirling fire plumes is pursued to understand how swirl alters the plume dynamics and combustion. One example is the ‘fire whirl’ which is known to arise naturally during forest fires. This buoyancy-driven fire plume entrains ambient fluid as heated gases rise. Vorticity associated with a mechanism such as wind shear can be concentrated by the fire, creating a vortex core along the axis of the plume. The result is a whirling fire. The current approach considers the relationship between buoyancy and swirl using a configuration based on fixing the heat release rate of the fire and imposing circulation. Large-eddy methodologies are used in the numerical analyses. Results indicate that the structure of the fire plume is significantly altered when angular momentum is imparted to the ambient fluid. The vertical acceleration induced by buoyancy generates strain fields which stretch out the flames as they wrap around the nominal plume centreline. The whirling fire constricts radially and stretches the plume vertically.

(Some figures in this article are in colour only in the electronic version; see [www.iop.org](http://www.iop.org))

### 1. Introduction

Fire whirls are a rare but potentially catastrophic form of fire. These swirling buoyant fire plumes are known to increase the danger of naturally occurring or post-disaster fires. Researchers have spent the last four decades investigating these devastating fires [1–5, 7, 8]. In order for a fire whirl to exist, there must be an organized source of angular momentum to produce the large swirl velocities as air is entrained into the fire plume [1, 2]. These vorticity-driven fires occur over a large range of length and velocity scales, and significantly alter the entrainment and combustion dynamics.

The earliest study to quantify a fire whirl from experiments was conducted by Emmons and Ying [1], who produced the phenomenon from a pool of acetone centred within a rotating cylindrical screen. They measured temperature profiles versus radius at a fixed height above the fuel for various values of imposed circulation. To extract mean temperature profiles from these data, they struggled to remove the effects of flame wander and averaged out turbulent fluctuations. From these reduced data, they determined the basic trend for circulation imposed on a buoyant plume: increasing circulation simultaneously reduces the mean radius and increases the mean temperature of the plume. Hence the flame lengthens vertically and tightens radially with increasing screen rotation. The physical explanation was that the vertical acceleration induced by buoyancy generates strain fields which stretch out the flames as they wrap around the nominal plume centreline. Unfortunately, Emmons and Ying did not provide data for the velocity fields produced by the flows.

§ Author to whom correspondence should be addressed.

A second significant study of buoyant plumes with circulation was carried out by Soma and Saito [3], who provided one set of instantaneous azimuthal velocity measurements as functions of radius at a specific height. To interpret the velocity measurements, they supposed that the flow is composed of an inviscid line vortex consisting of a rotating circular core where the velocity increases linearly with radius surrounded by a potential flow where the velocity falls off inversely with radius. Two constants determine this line vortex, its core radius and its strength, which Soma and Saito determined empirically to 3 cm and  $30 \text{ s}^{-1}$ , respectively. The curve, defined by the linear vortex model and the two experimentally deduced constants, seems to fit their data quite well.

In a third study, Satoh and Yang [4,5] examined fire whirls both experimentally and using numerical simulations (without a combustion model). In these studies, a flame was surrounded by a four-walled enclosure, opened at the top. Vertical gaps spanning the height of the enclosure were placed at each of the corner walls to induce swirl by channelling the entrained flow produced by the fire itself. The authors state that self-induced swirl is more realistic than externally imposed swirl for fire whirls generated by large urban or forest fires, and this is probably correct. However, their study does not allow the freedom to vary the ratio of circulation to buoyancy effects (as was done in the experiments of Emmons and Ying [1]), and no comparison is made to plume correlations in the absence of circulation to examine trends of the plume characteristics as the circulation is increased. To attempt to compare with Satoh and Yang's measurements, one must know the ratio of circulation to buoyancy effects induced by a fire in their enclosure under their experimental conditions; this information was not provided.

To the best of the authors' knowledge, these are the only studies which have presented quantitative, laboratory-scale data with which to compare a theory for buoyancy-driven flows with circulation. Other studies are also relevant, however. A review by Morton [2] describes the underlying mechanisms which produce and sustain a fire whirl. A mathematical description of a swirling buoyant plume arising from a point source of heat was developed by Thomas and Takhar [6]. Their analyses included cases for which circulation decays to zero outside of the plume or remains a finite constant. While the analysis of these cases showed qualitatively different behaviour, neither case would explain the observed plume dynamics found by Emmons and Ying [1]. Scale modelling is another approach to investigate fire whirls [3, 7, 8]. Williams [7] addressed the importance of scaling mass fires, Soma and Saito [3] developed scaling laws to model prototype fire whirls, and an intensive review of the fire spread scenarios has been reported by Hirano and Saito [8].

Other papers have examined the effects of circulation on momentum- and buoyancy-driven flows. Gabler *et al* [9] define whirling flames as a pure tangential motion and swirling flames as a combination of both axial and tangential motions of a flow. (We will not be concerned with these definitions in our study because all the axial motion is generated by the buoyancy flow field.) Chigier *et al* [10] replaced the liquid pool described by Emmons and Ying [1] with a turbulent jet diffusion flame. The experiments yielded increasing flame lengths with increasing rotation, increasing flow rates, or both. Tangirala and Driscoll [11] studied a fuel jet surrounded by coaxial swirling air. Increasing swirl decreased the flame, producing a short intense flame with improved stability, rapid mixing and increased temperatures. Increasing fuel jet momentum produced a more jet-like flame. Finally, Lee [12, 13] studied both theoretically and experimentally a buoyant swirling jet issuing into a quiescent ambient environment. He found that two dimensionless parameters characterizing the source governed the solution: a Froude number and a swirl parameter. His analysis for the swirling buoyant jet reduced to a non-swirling jet, a non-swirling plume or a swirling jet, when the governing parameters were chosen appropriately. Also, his experimental results seemed to confirm his theoretical

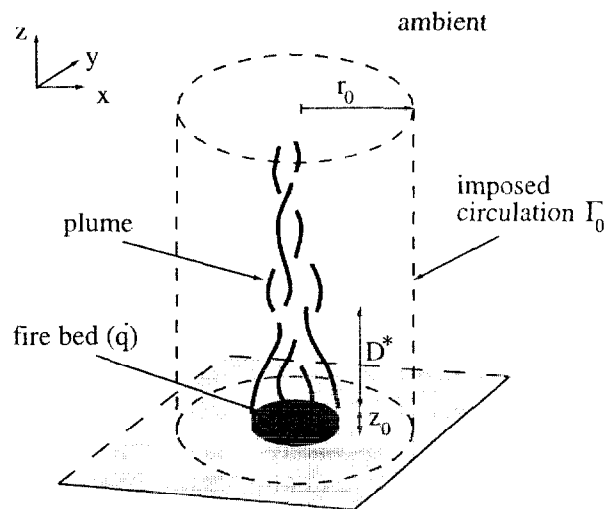


**Figure 1.** Schematic of a fire plume in ambient conditions under an imposed circulation  $\Gamma_0$  (e.g. a rotating cylindrical screen). The fire bed is of heat release rate  $\dot{q}$  with height  $z_0$  and flame height  $D^*$ .

predictions that forced, or momentum-driven flames behave differently from buoyancy-driven flames. Furthermore, it seems that flame lengths can decrease when mixing is enhanced and increase when mixing is suppressed.

To date, fire whirls have not been studied adequately either theoretically or experimentally. As previously noted, only three studies [1, 3, 4] have examined the phenomena experimentally in the laboratory. In this paper, we attempt to simulate numerically the phenomena observed in these experiments by imposing circulation into the ambient air on a buoyant plume. In this manner we can vary buoyancy and circulation independently and control the fundamental dynamics of swirling fire plumes. Furthermore, we hope that this presentation will stimulate more experimental study of this problem since clearly additional data on well characterized fire-driven, buoyant flows with circulation are needed.

In the absence of any swirl, the natural length scale for the fire is the flame height based on the overall heat release rate, ambient air properties and gravitational acceleration [14]. The problem can be made dimensionless based on this length scale together with the corresponding velocity and time scales so that the isolated plume depends only on a Reynolds number characterized by an effective kinematic viscosity. The imposed (swirl) circulation in these units characterizes the relative importance of swirl and buoyancy.

The experiments described above indicate three possible scenarios. First, the imposed circulation is held fixed, and the fire strength is allowed to change [1]. Second, the fire strength is fixed and the geometry determines the strength of the swirl [4]. Finally, both the imposed circulation and the fire strength can be specified, if a burner rather than a pool fire is used to generate buoyancy [10]. This last scenario can be considered as the ‘baseline’ fire whirl, whose dynamics are the subject of the present paper. Figure 1 is a schematic of the configuration. It is hoped that the constraints set by these simplifications can be relaxed systematically in future papers.

The paper is laid out as follows. Section 2 begins with a description of the mathematical models for the hydrodynamics and the combustion. Then the large-eddy simulation (LES) methodology is outlined. Section 3 is a presentation and discussion of the LES results for a fire plume without and with swirl. The discussion begins with a comparison of non-swirling

fires and well established plume correlations. Both non-swirling and swirling plumes are then contrasted to highlight basic physical differences. An important contribution of this paper is the presentation of temperature fields, swirl velocity characteristics and heat release rate trends with increasing circulation. The summary addresses the advantages and limitations of the simulations.

## 2. Methodology

### 2.1. Hydrodynamic model

The fire plume is a three-dimensional, transient, buoyant flow that can be modelled by the motion of a thermally expandable ideal gas [15]. The Navier–Stokes equations are solved for such a fluid driven by a prescribed heat source, where

$$\frac{\partial \rho}{\partial t} + \nabla \cdot \rho \mathbf{u} = 0 \quad (1)$$

$$\frac{\partial \rho Y_i}{\partial t} + \nabla \cdot \rho Y_i \mathbf{u} = \nabla \cdot \rho D_i \nabla Y_i + \dot{W}_i \quad (2)$$

$$\rho \left( \frac{\partial \mathbf{u}}{\partial t} + \mathbf{u} \cdot \nabla \mathbf{u} \right) + \nabla p - \rho \mathbf{g} = \nabla \cdot \boldsymbol{\tau} \quad (3)$$

$$\frac{\partial \rho h}{\partial t} + \nabla \cdot \rho h \mathbf{u} - \frac{d p_0}{d t} = \dot{q}''' + \nabla \cdot \left( k \nabla T + \sum \rho h_i D_i \nabla Y_i + \dot{q}_R \right) \quad (4)$$

$$p_0(t) = \rho T \mathcal{R} \sum (Y_i / M_i). \quad (5)$$

The fluid variables are the density  $\rho$ , velocity  $\mathbf{u}$ , mass fraction of the  $i$ th species  $Y_i$ , mass diffusivity of the  $i$ th species  $D_i$ , production rate of the  $i$ th species  $\dot{W}_i$ , pressure  $p$ , gravity  $\mathbf{g}$ , viscous stress tensor  $\boldsymbol{\tau}$ , enthalpy  $h$ , volumetric heat release rate  $\dot{q}'''$ , thermal conductivity  $k$ , temperature  $T$ , radiant energy flux  $\dot{q}_R$ , universal gas constant  $\mathcal{R}$  and molecular weight of the  $i$ th species  $M_i$ .

The pressure is decomposed into three components, a background (average) pressure  $p_0(t)$ , a hydrostatic contribution  $-\rho_0 g z$  and a perturbation to the hydrostatic  $\tilde{p}(\mathbf{x}, t)$ . The subscript 0 is a reference value of density and  $z$  is the vertical coordinate. Equations (4) and (5) are modified using the background pressure  $p_0$  which depends on time  $t$  only. In this manner, high-frequency acoustic oscillations are eliminated while large temperature and density variations typically found in fires are retained. The resulting equations are referred to as weakly compressible and are valid for low Mach number flows [15].

A further assumption is that the constant-pressure specific heat of the  $i$ th species  $c_{p,i}$  is independent of temperature. Therefore, the enthalpy is written as

$$h = \sum h_i Y_i = T \sum c_{p,i} Y_i.$$

Combining the conservation equations for mass (1), energy (4) and state (5) results in an expression for the divergence of the flow  $\nabla \cdot \mathbf{u}$ ,

$$p_0(t) \nabla \cdot \mathbf{u} + \frac{1}{\gamma} \frac{d p_0}{d t} = \frac{\gamma - 1}{\gamma} \left[ \dot{q}''' + \nabla \cdot \left( k \nabla T + \sum \rho h_i D_i \nabla Y_i + \dot{q}_R \right) \right]. \quad (6)$$

The term  $\nabla \cdot \mathbf{u}$  is an important quantity that is later exploited in the numerical solution. Equation (6) is integrated over the entire domain for pressure  $p_0$  and is used as a consistency condition.

The momentum equation (3) is simplified by subtracting off the hydrostatic pressure gradient, and then dividing by the density to obtain

$$\frac{\partial \mathbf{u}}{\partial t} + \frac{1}{2} \nabla |\mathbf{u}|^2 - \mathbf{u} \times \boldsymbol{\omega} + \frac{1}{\rho_0} \nabla \tilde{p} = \frac{1}{\rho} ((\rho - \rho_0) \mathbf{g} + \nabla \cdot \boldsymbol{\tau})$$

where  $\boldsymbol{\omega}$  is the vorticity. The head  $\mathcal{H}$  is introduced, where

$$\nabla \mathcal{H} \equiv \frac{1}{2} \nabla |\mathbf{u}|^2 + \frac{1}{\rho_0} \nabla \tilde{p}.$$

The final form of the momentum equation is

$$\frac{\partial \mathbf{u}}{\partial t} - \mathbf{u} \times \boldsymbol{\omega} + \nabla \mathcal{H} = \frac{1}{\rho} ((\rho - \rho_0) \mathbf{g} + \nabla \cdot \boldsymbol{\tau}). \quad (7)$$

The quantity  $1/\rho_0$  implies that the vorticity generation induced by buoyancy is much more important than that due to baroclinic effects, i.e. the non-alignment of the pressure and density gradients. This approximation, while excellent away from the combustion zone, is less so where heat release is significant [16]. As shown in [16], within the combustion zone, both non-buoyant baroclinic vorticity and buoyancy-induced vorticity are comparable. However, outside the combustion zone, the buoyancy-induced vorticity dominates and is the largest contribution to the vorticity overall. Since the solenoidal component of the velocity field is related to the vorticity through an elliptic equation, i.e. the Biot–Savart law, the solenoidal velocity, whether inside or outside the combustion region, is determined by the accumulative effect of the vorticity everywhere. Hence, the solenoidal component of the velocity field is dominated by the buoyancy-induced vorticity as assumed.

The equations presented thus far can be solved directly to obtain a solution to the problem of a buoyant fire plume. The difficulty arises in that the length and time scales associated with the fluid dynamics and combustion vary over orders of magnitude. In order to calculate the dynamics of the problem, models for  $\boldsymbol{\tau}$  and  $\dot{q}'''$  are necessary. The goal is to capture mixing on scales where the eddy viscosity is effective which generally requires a very fine grid to resolve the scales. An alternative approach is to use an elaborate sub-grid scale description. One representation of the dynamic viscosity is based on the analysis of Smagorinsky [17] where the sub-grid scale Reynolds stress tensor is given by

$$\tau_{ij} = \mu \left( \frac{\partial u_i}{\partial x_j} + \frac{\partial u_j}{\partial x_i} - \delta_{ij} \frac{2}{3} \frac{\partial u_k}{\partial x_k} \right) \quad \mu = \rho (C_s \Delta)^2 |S|$$

where  $C_s$  is an empirical constant,  $\Delta$  is a length on the order of the grid cell size and

$$|S|^2 = 2 \left( \frac{\partial u}{\partial x} \right)^2 + 2 \left( \frac{\partial v}{\partial y} \right)^2 + 2 \left( \frac{\partial w}{\partial z} \right)^2 + \left( \frac{\partial u}{\partial y} + \frac{\partial v}{\partial x} \right)^2 + \left( \frac{\partial u}{\partial z} + \frac{\partial w}{\partial x} \right)^2 + \left( \frac{\partial v}{\partial z} + \frac{\partial w}{\partial y} \right)^2.$$

There have been numerous refinements of the original Smagorinsky model, but it is difficult to assess the improvements offered by these newer schemes. There are two reasons for this. First, the structure of the fire plume is dominated by the large-scale resolvable eddies so that even a constant eddy viscosity gives results almost identical with those obtained with the Smagorinsky scheme [18]. Second, the lack of precision in most large-scale fire data makes it difficult to sort out the subtleties associated with these models. For the time being, the Smagorinsky model with  $C_s = 0.14$  produces satisfactory results for most large-scale applications where boundary layers are not important.

The pressure perturbation is solved by taking the divergence of the momentum equation which results in an elliptic partial differential equation for  $\mathcal{H}$

$$\nabla^2 \mathcal{H} = -\frac{\partial(\nabla \cdot \mathbf{u})}{\partial t} - \nabla \cdot \mathbf{F} \quad (8)$$

where the convective and diffusive terms have been incorporated in the term  $\mathbf{F}$ .

## 2.2. Combustion model

For the large-eddy simulations, a sub-grid thermal element model (TEM) is formulated to represent the fire. A large number of Lagrangian particles are introduced into the plume, releasing heat as they are convected by the thermally induced motion [19, 20]. The combustion and hydrodynamics are coupled since the fluid motion determines where the heat is released, while the heat release determines the motion. The concept is based on mixture-fraction theory for the transport of a conserved scalar that describes a reacting species. The TEM requires that the burning rate be prescribed as an input into the calculation. It is intended for applications where small-scale mixing and diffusive processes that control non-premixed combustion cannot be resolved on the grid used to perform the simulation. In our computation, the combustion is modelled by a simple single-step reaction: fuel and oxygen combine to produce product. Only fuel and oxygen are tracked in the simulations.

The overall heat release rate  $\dot{q}$  from the fire is discretized as thermal elements that represent pyrolyzed fuel. At a specified surface, such as the fuel bed, thermal elements are ejected at a rate of  $\dot{n}''$  particles per unit time per unit area with a small normal velocity into the flow domain. The heat release rate of a single thermal element is given by

$$\dot{q}_{p,j} = \frac{\dot{q}''}{\dot{n}''} \frac{1}{t_b} \quad (t - t_0 < t_b)$$

where  $\dot{q}''$  is the heat release rate per unit area of the fuel bed and  $t_b$  is the burn-out time of the thermal element. The burn-out time is obtained from the plume correlations of Baum and McCaffrey [14]. It is assumed that the thermal element burns out somewhere in the intermittent region of the plume,  $1.32D^* < z < 3.30D^*$ , where  $z$  is the height above the fire bed,  $D^* = [\dot{q}/(\rho_0 c_p T_0 \sqrt{g})]^{2/5}$  is the characteristic diameter of the fire, and  $\dot{q}$  is the total heat release rate of the fire. The burn-out time falls somewhere between  $1.05\sqrt{D^*/g} < t_b < 1.86\sqrt{D^*/g}$  and is usually a few tenths of a second. The heat release term in (4) is the summation of convective heat release rates of the individual thermal elements in a grid cell of volume  $\delta x \delta y \delta z$ .

$$\dot{q}''' = \frac{\sum \dot{q}_{p,j}}{\delta x \delta y \delta z}$$

For the inclusion of oxygen transport in the calculation, the burn-out time of any thermal element will vary based on the concentration of oxygen in the surrounding gas. Oxygen is consumed in any given control volume based on the amount of heat generated in the control volume. The source term in the oxygen transport equation (2) becomes

$$\dot{W}_{O_2} = -\frac{\dot{q}'''}{\Delta H_{O_2}}$$

where  $\Delta H_{O_2}$  is the amount of heat liberated per unit mass of oxygen consumed (usually about  $13\,100 \text{ kJ kg}^{-1} \text{ O}_2$ ). When the oxygen mass fraction  $Y_{O_2}$  falls to a certain prescribed lower limit, combustion is assumed to stop, and the unburned fuel associated with the thermal elements remains unburned until more oxygen is available. In general, if the number of burning particles

exceeds the number of grid cells in which they reside, results do not depend upon the number of particles used for the simulation. The totality of these particles determines the oxygen sinks [21], obviating the need for sub-grid scale resolution of the combustion processes. The only quantities tracked then are the fuel particles and the oxygen concentration on the Eulerian grid, as described above.

### 2.3. Numerical formulation

The equations solved numerically are the conservation of mass (1), species (2), momentum (3) and the Poisson equation for the total pressure which is formulated from the energy equation (4) and state equation (5). The combustion is simulated via the thermal element model as described in section 2.2. The spatial derivatives are discretized with second-order central differencing, and a second-order explicit Runge–Kutta scheme is used to advance the velocity and temperature fields. The linear algebraic system arising from the discretization of the Poisson equation (8) has constant coefficients and can be solved to machine accuracy by direct (non-iterative) methods that utilize fast Fourier transforms and block tri-diagonal solvers. The grid is rectangular with uniform spacing in the horizontal directions and stretching in the vertical direction. The discretization for a computational cell is based on staggered-gridding techniques.

No-flux boundary conditions are specified by asserting that

$$\frac{\partial \mathcal{H}}{\partial n} = -F_n$$

at solid walls, where  $F_n$  is the normal component of  $F$  at the wall. Therefore, the normal component of velocity at the wall does not change with time, and indeed remains zero assuming that the flow velocity is initially zero. At open external boundaries it is assumed that the perturbation pressure is zero. Thermal elements are ejected from the burner surface and burn according to the heat release rate per unit area  $\dot{q}''$  which is specified as an input. An adiabatic boundary condition is used so that there is no temperature gradient normal to the burner surface. Refer to McGrattan *et al* [19] for further details.

### 3. Large-eddy simulations

The simulations of a whirling fire are based on the schematic shown in figure 1. The domain is a rectangular region with a square base 0.50 m per side and a 1.0 m height. A circular burner is centred at the base of the domain with diameter  $d = 0.0863$  m and height  $z_0 = 0.05$  m. The origin of the Cartesian coordinate system is centred at the base. The burner specifications represent a fuel source of acetone yielding a 14.4 kW fire. The oxygen transport model was used with a prescribed mass fraction burnout of 0.15.

Analogous to the experiments of Emmons and Ying [1], swirl can be induced by simulating an imposed circulation  $\Gamma_0$  on the fire plume at a prescribed radial distance  $r_0$  from the nominal centreline. Three dimensionless parameters govern the flow generated by this model:

- (a) the heat-release rate  $\dot{q}$  made dimensionless using thermal properties of the ideal gas;
- (b) the circulation made dimensionless using a characteristic flame diameter  $D^*$  [14] and buoyant velocity  $\sqrt{gD^*}$ , where  $\Omega/\alpha = (\Gamma_0/2\pi r_0^2)/\alpha$ ;
- (c) a Reynolds number based on the buoyant velocity and flame diameter.

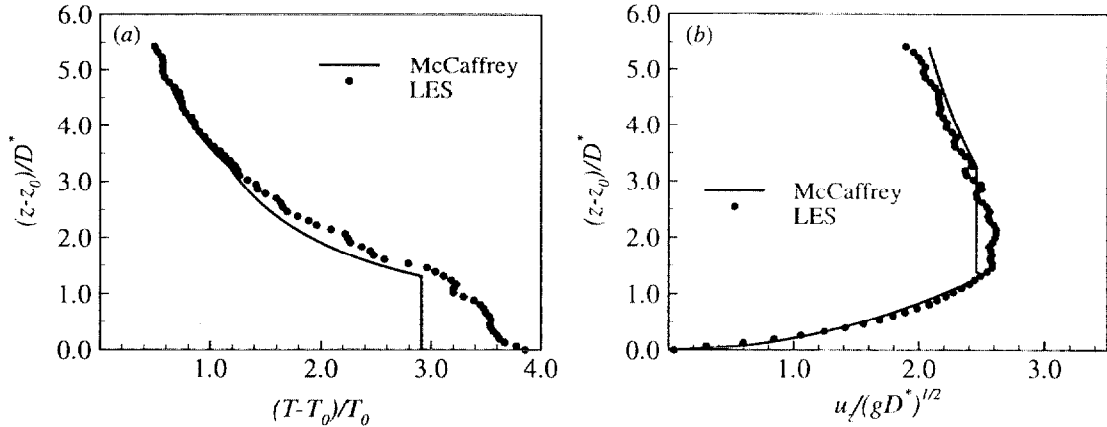


**Figure 2.** Comparison of the McCaffrey correlations [14] with LES for the time-averaged centreline (a) temperature and (b) vertical velocity.

The parameter  $\alpha$  is the reciprocal of a time scale which characterizes the flame strain due to buoyancy  $\alpha = \sqrt{g/D^*}$ . Therefore, the parameter  $\Omega/\alpha$  provides a measure of the effects of swirl-induced motion to buoyancy-driven motion. The Reynolds number is defined using the characteristic parameters most relevant to the described problem. However, its definition should not be confused with the dynamic Reynolds number of the large-scale simulations (refer to section 2.1). Additional dimensionless parameters are the ratio of length scales  $r_0/D^*$  and  $d/D^*$ ; note that for these simulations the parameters are fixed and of order unity.

Results are presented for the large-eddy simulations using a rectangular grid. Numerical tests were performed to determine the grid size necessary to resolve the flow field with the best accuracy. Five mesh sizes ranging from  $32^3$  cells to  $128^3$  cells were used in the analysis. Based on *Richardson's extrapolation*, simulations calculated on a  $72^3$  grid (consisting of 373 248 cells) yield a relative error of about 4%. An average simulation takes approximately  $18 \mu\text{s}$  per time step per cell on an SGI Octane/SI R10000 195 MHz processor†, and requires about 12 000 time steps for 20 s of simulation time.

The LES model was found to reproduce mean temperature and buoyant velocity correlations for large fire plumes in the absence of circulation over most of the simulated domain. Figures 2(a) and (b) compare the simulations with the McCaffrey correlations for the time-averaged centreline temperature and vertical velocity, respectively. Baum and McCaffrey [14] define three major zones for a typical fire plume. The zones are referred to as (a) the continuous (visible) flame for  $0 < (z - z_0)/D^* < 1.32$ , (b) the intermittent region for  $1.32 \leq (z - z_0)/D^* \leq 3.30$  and (c) the plume region for  $3.30 < (z - z_0)/D^*$ . Time-averaged radial temperature and velocity profiles have been shown previously by Baum *et al* [18]. The good correspondence between the correlation data and the simulations is very encouraging, and provides confidence for the LES formulation.

However, it is worthwhile to note that near the base of the fire the correspondence between the temperature correlations and LES deviates. The discrepancy is not a failure of the correlations but is a limitation of the current model. Neither the correlations nor the numerical model were constructed to apply near the base of a fire, but rather serve as a global description of flow dynamics. There is presently insufficient consensus between experiments to properly guide the formulation of a model to represent the entrainment region close to the fuel source

† The computer is identified to specify the computational timings and is not intended to imply recommendation or endorsement by NIST.

[22]. The reason for this is twofold: (a) the region near the base of the fire is sensitive to the fuel geometry and can change drastically depending on the boundary conditions, experimental apparatus, etc, and (b) there is great uncertainty in the measurements of entrainment rates near the fuel source due to localized effects.

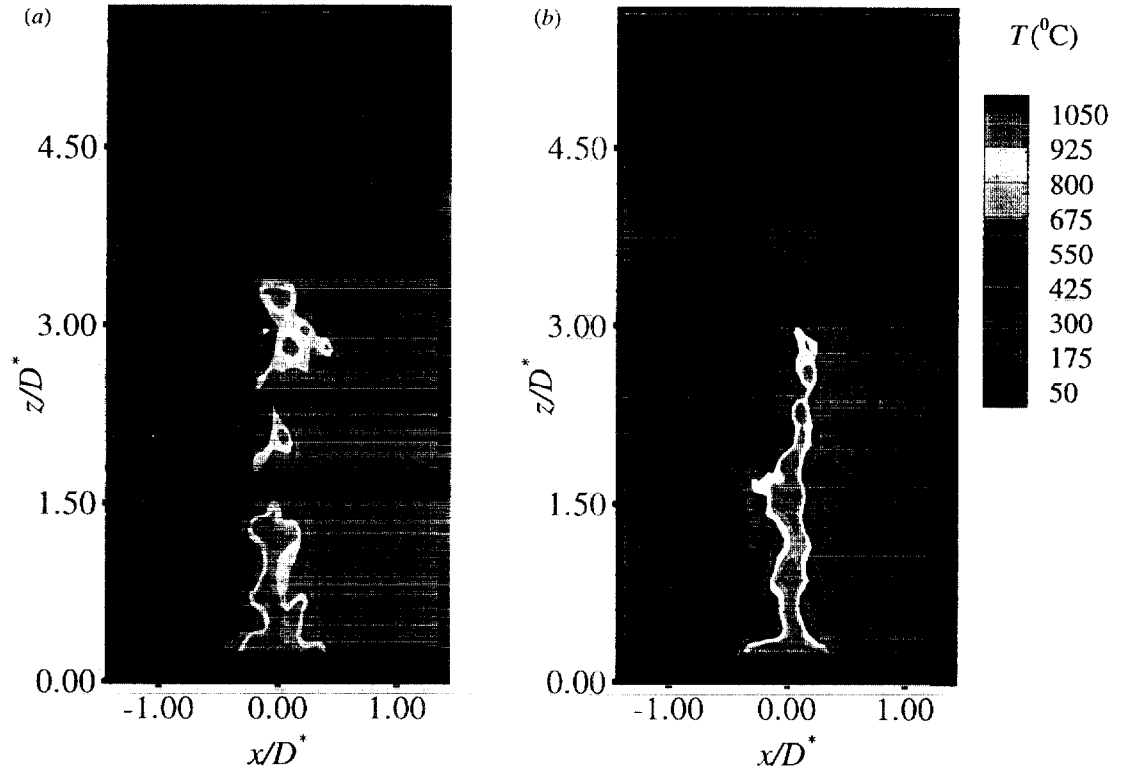
The fire plume was simulated with an imposed circulation at a distance  $r_0 = 0.2$  m measured from the nominal plume centre and along the entire height of the domain. A comparison of the instantaneous temperature fields for a non-swirling ( $\Omega/\alpha = 0.0$ ) and swirling fire ( $\Omega/\alpha = 0.536$ ) is shown in figures 3(a) and (b), respectively. The non-swirling flame in figure 3(a) shows the onset of characteristic puffing associated with a typical fire [18, 23] as two hot regions near  $z/D^* = 0.5$  and 1.0. However, the swirling fire (figure 3(b)) tends to have a continuous flame up to  $z/D^* = 2.3$ . Another difference is that the temperature contours shown in figure 3(b) define the continuous flame as being more tapered and constricted near the centreline than the non-swirling flame. Contours of heat release rate per unit volume  $\dot{q}'''$  are shown in figures 4(a) and (b) for  $\Omega/\alpha = 0.0$  and 0.536. Note that the swirling fire has more regions of high heat release rate than the non-swirling fire.

A three-dimensional representation of the two cases is shown in figures 5(a) and (b). The figures are isotherms for three temperature levels corresponding to the different plume regimes defined previously. Sample Lagrangian trajectories are shown as ribbons which follow the path of a streamline. The trajectory of figure 5(a) shows how a particle entrained in the non-swirling fire is drawn towards the centre of the plume and then merely travels straight up. A particle entrained in a swirling fire is also drawn towards the centre of the plume but wraps around the plume a few times near the base of the fire before accelerating vertically. The general fluid motion of a swirling fire is unstable, as the fire typically oscillates or precesses within the boundaries of the fire bed. Bearing this in mind, time-averaged data are now presented.

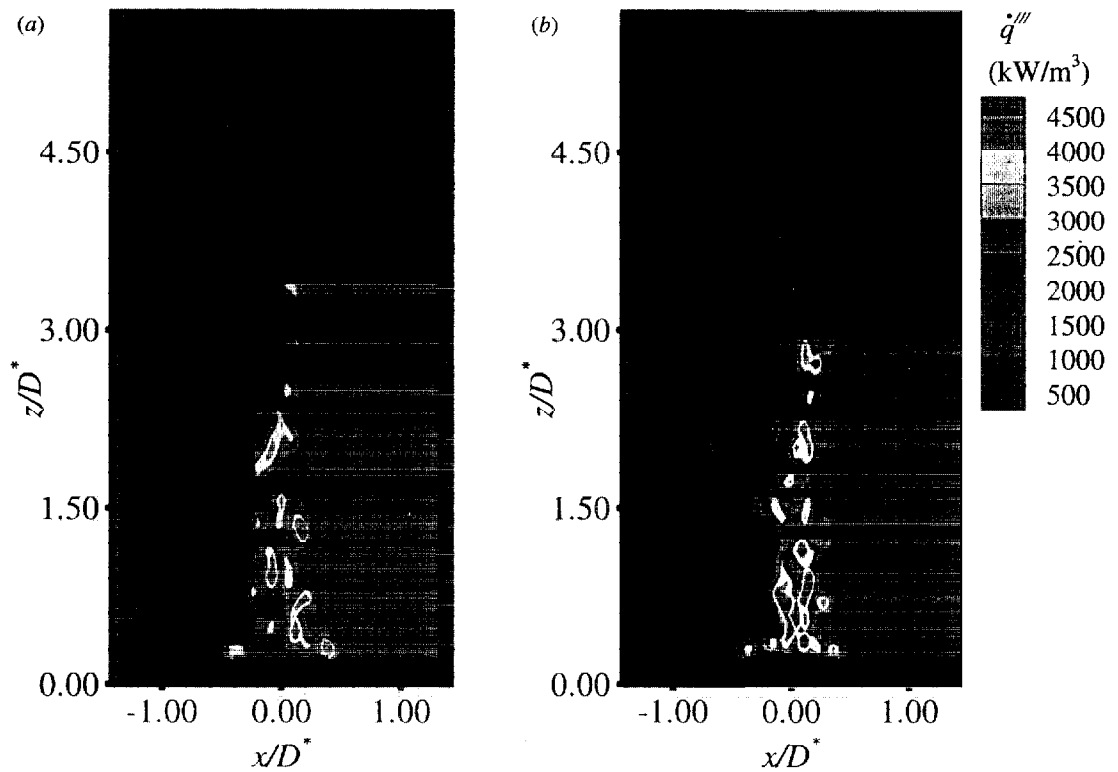
The time-averaged temperature fields shown in figures 6(a) and (b) are not as elucidating as the instantaneous fire images (figures 3(a) and (b)). The temperature contours of the non-swirling fire (figure 3(a)) are more symmetric than the swirling fire (figure 3(b)). It appears that time-averaging smears out the precessing motion of the swirling flows. However, to draw comparisons with experimental work, the remainder of this paper will consider results for the mean flow fields.

Figure 7 shows six cases of the time-averaged temperature fields for values of circulation from  $\Omega/\alpha = 0.0$  to  $\Omega/\alpha \sim 0.8$ . At first, increasing the circulation results in a larger region of high temperatures near the fire bed. The simulations then predict that further increasing the circulation above  $\Omega/\alpha > 0.268$  reduces the region of high temperatures. However, the isotherms near the central region of the plume show that the flame has narrowed and stretched vertically for  $\Omega/\alpha \geq 0.536$ . The flame-lengthening trends discussed by Chigier *et al* [10] are qualitatively similar to that reported here. Furthermore, there is very good agreement when cases  $\Omega/\alpha = 0.0$  and 0.804 (figure 7) are compared with the temperature distributions of the propane diffusion flame [10], for both flame shape and temperature ranges.

Another way to interpret the varying effects of circulation is shown as contours of time-averaged heat release rate per unit volume in figure 8. Increasing the circulation reduces the overall volume of the fire plume and increases the region of high heat release rates within the central region of the flame. The heat release rate contours near the base for  $\Omega/\alpha > 0.50$  have two peaks and a small dip near the centreline, which seems to be a consequence of time averaging an oscillating flow. The experimental observations of Emmons and Ying [1] indicate that the heat release rate is significantly increased by the swirling motion. Although the numerical methodology described in section 2 does not model varying heat release rate, it is very encouraging that the simulated results show larger regions of higher heat release rates.



**Figure 3.** Instantaneous temperature field at the plume centre-plane for: (a) non-swirling fire  $\Omega/\alpha = 0.0$  and (b) whirling fire  $\Omega/\alpha = 0.536$ .



**Figure 4.** Instantaneous heat release rate per unit volume at the plume centre-plane for (a) non-swirling fire  $\Omega/\alpha = 0.0$ , and (b) whirling fire  $\Omega/\alpha = 0.536$ .

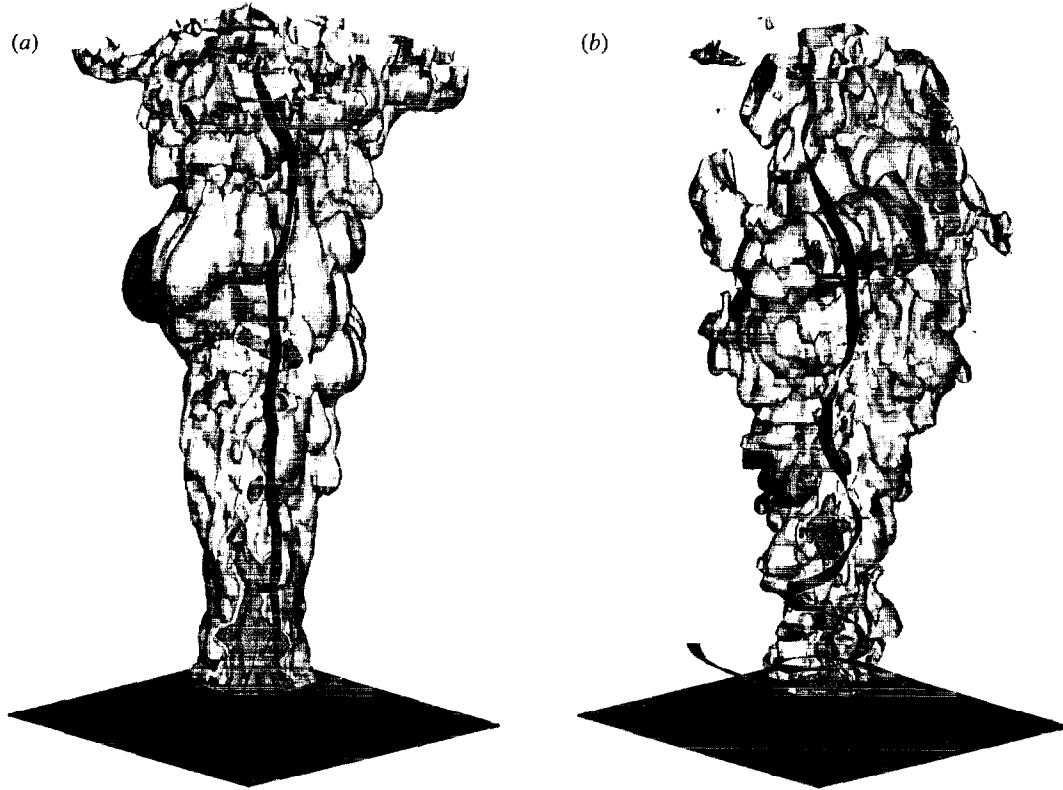


Figure 5. Simulations of a plume for: (a) non-swirling fire  $\Omega/\alpha = 0.0$ , (b) whirling fire  $\Omega/\alpha = 0.536$ . Isotherms are shown for three major zones: the continuous flame (red), the intermittent region (yellow) and the plume region (grey). The blue ribbons are sample Lagrangian trajectories of the flow fields.

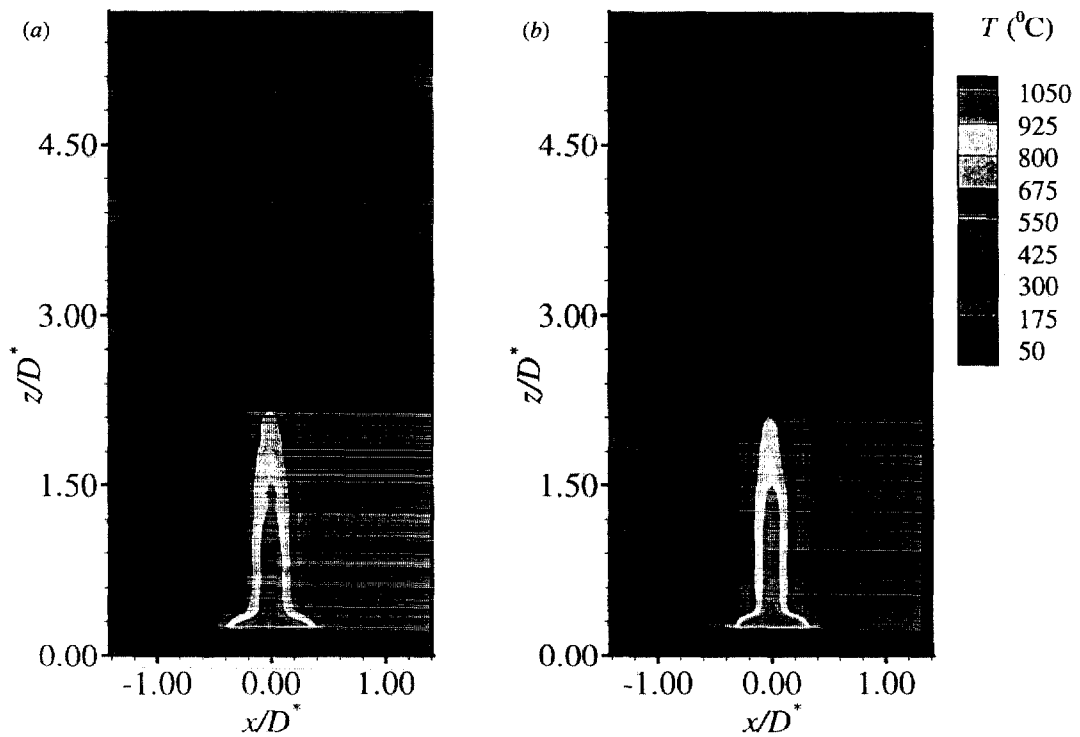


Figure 6. Time-averaged temperature fields at the plume centre-plane for: (a) non-swirling fire  $\Omega/\alpha = 0.0$  and (b) whirling fire  $\Omega/\alpha = 0.536$ .

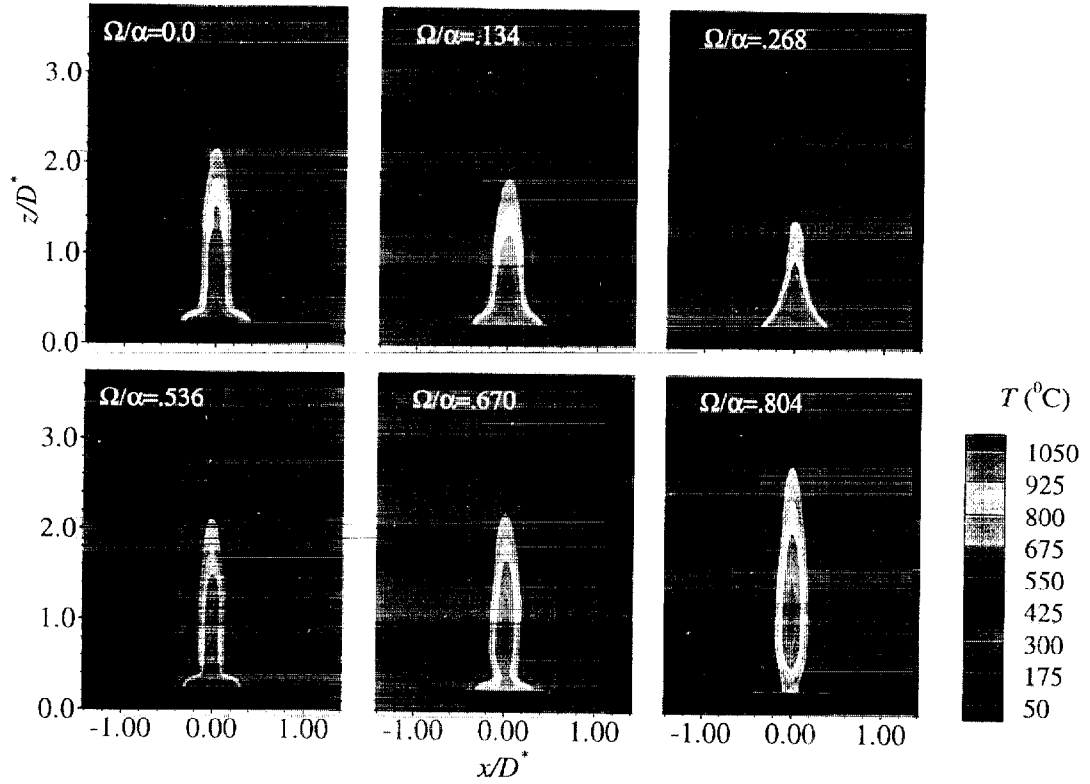


Figure 7. Time-averaged temperature fields at the plume centre-plane for varying circulation  $\Omega/\alpha$ .

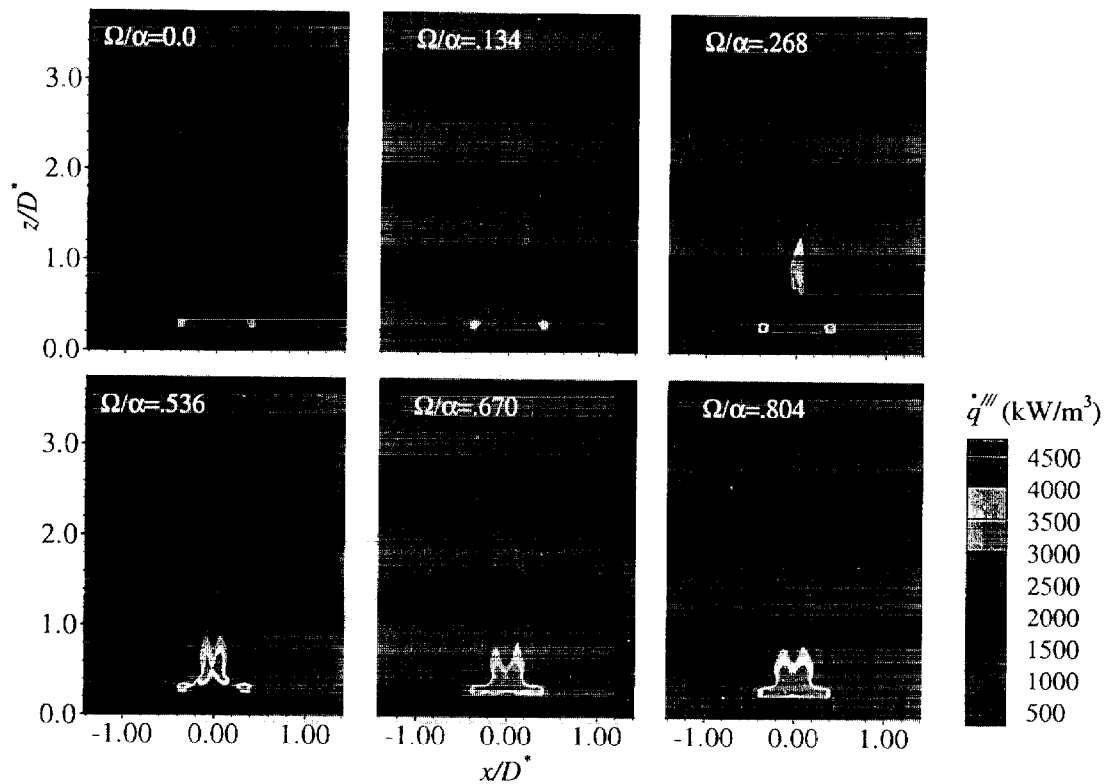


Figure 8. Time-averaged heat release rate per unit volume at the plume centre-plane for varying circulation  $\Omega/\alpha$ .

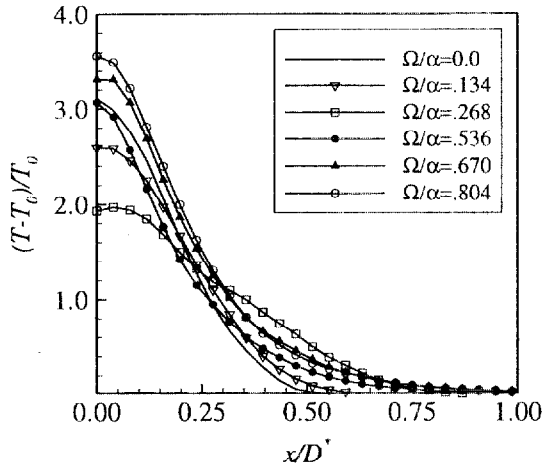


Figure 9. Mean temperature profiles at  $(z - z_0)/D^* = 1.5$  for varying circulation.

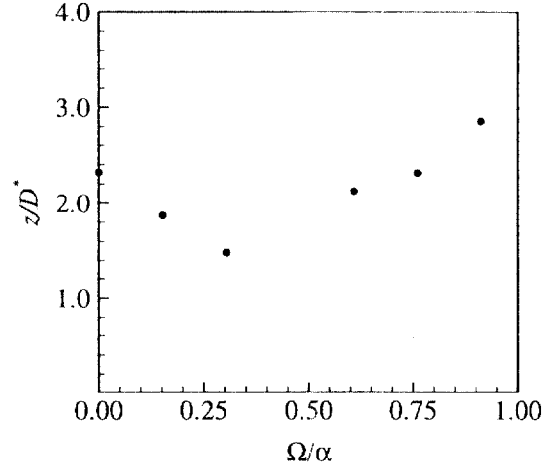


Figure 10. Mean centreline flame height (based on  $925^\circ\text{C}$ ) versus circulation.

Time-averaged temperature profiles for the six cases of circulation are shown in figure 9 at  $(z - z_0)/D^* = 1.5$ . Overall, the temperature profiles have nearly the same distribution along  $x$  at the centre-plane. A closer examination of the temperatures near the centreline ( $x = 0.0$ ) reveals an interesting pattern. Initially, the mean temperature at the centreline reduces with increasing circulation up to  $\Omega/\alpha = 0.536$ . Further increasing circulation then results in an increase of the mean temperature at the centreline. The decreasing/increasing temperature trends are also reflected in figure 7 of time-averaged isotherms.

At this point we explore the possibility of defining a characteristic flame height for the six cases presented. According to analyses of Orloff and de Ris [24], the size and shape of pool fires can be constructed through Froude modelling. Their model was substantiated with experimental data from pool fires of various fuels. The luminous flame volume was defined by an effective flame temperature of  $1200\text{ K}$  (independent of fuel) for which the Froude modelling suggested an average volumetric heat release rate of  $1200\text{ kW m}^{-3}$ . Returning to figure 7, the flame height can be visualized as the contour marking  $925^\circ\text{C}$ . Likewise, figure 8 delineates the flame shape between contours  $1000\text{--}1500\text{ kW m}^{-3}$ . A characteristic mean flame height at the centreline based on  $925^\circ\text{C}$  is shown in figure 10 to re-emphasize the decreasing/increasing flame height trends previously discussed.

The numerical simulations can be compared to the experimental findings of Emmons and Ying [1]. Their study of a fire whirl included temperature profiles for different values of circulation. The experimental trends indicate that with increasing circulation, the maximum mean temperature peaked off-centre. Figures 11(a) and (b) are mean temperature profiles for  $\Omega/\alpha = 0.0$  and  $0.536$ . The maximum mean temperature for the non-swirling fire always occurs at the plume nominal centreline and decreases with height. In the case of the swirling fire, the maximum temperatures also occurred at the nominal centreline. Further data analyses indicated that, depending on the number of realizations captured in one complete revolution of the fire, the time-averaged data may yield asymmetric features of the flow. It is not clear whether the off-centreline peak temperatures as reported in [1] are an artefact of the oscillating motion of the fire or due to the location of the flame sheet.

The swirl velocity profiles provide further information regarding the fluid motion. The time-averaged profiles are shown in figure 12 for varying circulation at position  $(z - z_0)/D^* = 1.5$ . In the absence of circulation, the mean swirl velocity is approximately zero with some

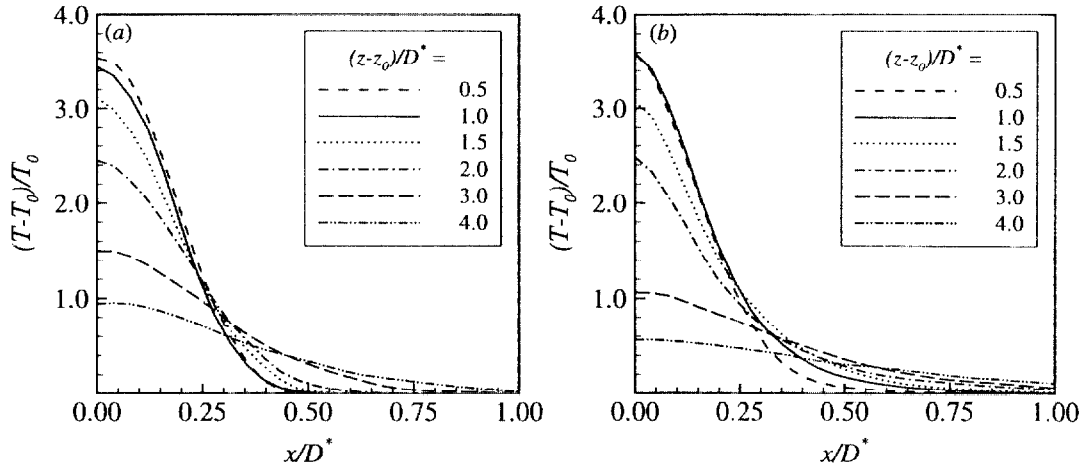


**Figure 11.** Time-averaged temperature profiles for: (a) non-swirling fire  $\Omega/\alpha = 0.0$  and (b) whirling fire  $\Omega/\alpha = 0.536$ , for varying height  $(z - z_0)/D^*$ .

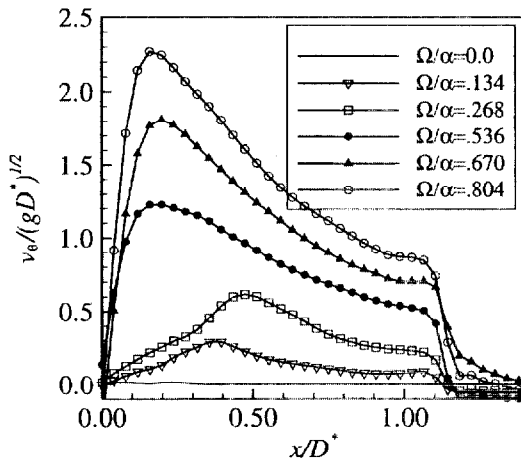


**Figure 12.** Mean swirl velocity profiles at  $(z - z_0)/D^* = 1.5$  for varying circulation.

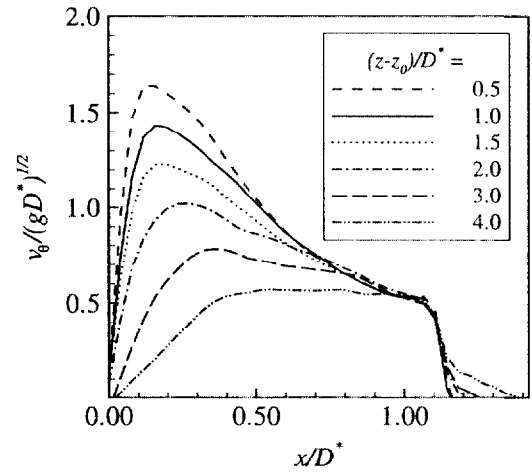


**Figure 13.** Mean swirl velocity profiles of whirling fire  $\Omega/\alpha = 0.536$  for varying height.

fluctuation near the plume centreline and closest to the fire bed. Once circulation is introduced, the magnitude of the swirl velocity increases with increasing circulation. Peak values of swirl velocity occur at  $x/D^* \sim 0.4$ , which corresponds to the edge of the burner and may be indicative of high heat release rates near the edge of the flame. Beyond  $x/D^* = 1.1$ , the position at which circulation is imposed, the swirl velocity decays to zero. Figure 13 is a plot of the mean swirl velocity versus  $x/D^*$  at various heights for  $\Omega/\alpha = 0.536$ . The curves indicate that the peak swirl velocity decreases with increasing height  $z$ . As the plume spreads radially, the swirl velocities tend to mix outward and reduce the swirl velocities, suggesting that buoyancy increasingly dominates the dynamics further up the plume.

#### 4. Concluding remarks

Numerical simulations of fire plumes were conducted in order to ascertain the dynamic attributes of swirl and buoyancy in whirling fires. The LES methodology for simulating fires is based on a direct solution of the large scales and sub-grid scale approximations for

the dynamic viscosity and heat release. The simulations for non-swirling fires are in very good agreement with mean temperature and buoyant velocity correlations for large fires. The approach taken for swirling fires was to impose circulation while maintaining a constant heat release rate.

It was shown that increasing circulation has a strong influence on the shape of the fire plume. The whirling fires increased in length and constricted radially, consistent with previously published literature. The temperature trends along the centreline decreased and then increased in value for increasing circulation. Despite the fixed heat release, increasing circulation increased the region of maximum heat release rates while reducing the overall volume of the fire. The swirl velocities also increased with increasing swirl. In addition, it was determined that further up the plume buoyancy effects are more dominant than the swirl velocities.

The present study carefully explored the effects of circulation on a fire plume. The scenario of a fixed fire strength and variable circulation was the first numerical study to systematically analyse the relationship between swirl and buoyancy. A set of well defined experiments to match the current numerical approach will be beneficial for a more quantitative comparison and validation. The next step will be to relax the condition of a fixed heat release to one that varies according to the radiation heat feedback to the surface of the fire. This, in itself, changes the current problem of an imposed fuel flow to a pool fire.

### Acknowledgments

This research was supported by a National Research Council Postdoctoral Fellowship. We wish to thank the reviewers for their thoughtful and helpful comments and suggestions. The first author is grateful for helpful discussions with Dr William (Ruddy) Mell during the course of this research. This manuscript is dedicated to the pioneering work of Professor H W Emmons (1912–98).

### References

- [1] Emmons H W and Ying S J 1967 *Proc. 11th Int. Symp. on Combustion* (Pittsburgh, PA: Combustion Institute) pp 475–88
- [2] Morton B R 1970 *Fire Res. Abs. Rev.* **12** 1–19
- [3] Soma S and Saito K 1991 *Combust. Flame* **86** 269–84
- [4] Satoh K and Yang K T 1996 *ASME Heat Trans. Div.* **335** 393–400
- [5] Satoh K and Yang K T 1997 *Proc. 5th Int. Symp. on Fire Safety Science* pp 201–12
- [6] Thomas T G and Takhar H S 1988 *Acta Mech.* **71** 185–93
- [7] Williams F A 1982 *Prog. Energy Combust. Sci.* **8** 317–54
- [8] Hirano T and Saito K 1994 *Prog. Energy Combust. Sci.* **20** 461–85
- [9] Gabler H C, Yetter R and Glassman I 1998 *Proc. 34th AIAA/ASME/SAE/ASEE Joint Propulsion Conf.* AIAA Paper 98-3530 pp 1–11
- [10] Chigier N A, Beér J M, Grecov D and Bassindale K 1970 *Combust. Flame* **14** 171–80
- [11] Tangirala V and Driscoll J F 1988 *Combust. Sci. Technol.* **60** 143–62
- [12] Lee Shao-Lin 1966 *Trans. ASME, J. Appl. Mech.* **33** 647–55
- [13] Lee Shao-Lin 1966 *Trans. ASME, J. Appl. Mech.* **33** 656–61
- [14] Baum H R and McCaffrey B J 1989 *Proc. 2nd Int. Symp. on Fire Safety Science* pp 129–48
- [15] Rehm R G and Baum H R 1978 *J. NBS Res.* **83** 297–308
- [16] Mell W E, McGrattan K B and Baum H R 1996 *Proc. 26th Int. Symp. on Combustion* (Pittsburgh, PA: Combustion Institute) pp 1–14
- [17] Smagorinsky J 1963 *Mon. Weather Rev.* **91** 99–164
- [18] Baum H R, McGrattan K B and Rehm R G 1997 *Proc. 5th Int. Symp. on Fire Safety Science* pp 511–22
- [19] McGrattan K B, Baum H R and Rehm R G 1998 *Fire Safety J.* **30** 161–78

- [20] Baum H R, Ezekoye O A, McGrattan K B and Rehm R G 1994 *Theoretical and Computational Fluid Dynamics* **6** 125–39
- [21] Huggett C 1980 *Fire J. Mater.* **4** 61–5
- [22] Zhou X C, Gore J P and Baum H R 1996 *Proc. 26th Int. Symp. on Combustion* (Pittsburgh, PA: Combustion Institute) pp 1453–9
- [23] Cetegen B M and Ahmed T A 1993 *Combust. Flame* **93** 157–84
- [24] Orloff L and de Ris J 1982 *Proc. 19th Int. Symp. on Combustion* (Pittsburgh, PA: Combustion Institute) pp 885–95